

## Photonic bandgap narrowing in conical hollow core Bragg fibers

Fahri Emre Ozturk, Adem Yildirim, Mehmet Kanik, and Mehmet Bayindir

Citation: *Applied Physics Letters* **105**, 071102 (2014); doi: 10.1063/1.4893594

View online: <http://dx.doi.org/10.1063/1.4893594>

View Table of Contents: <http://scitation.aip.org/content/aip/journal/apl/105/7?ver=pdfcov>

Published by the [AIP Publishing](#)

---

### Articles you may be interested in

[Chemical sensing by differential thermal analysis with a digitally controlled fiber optic interferometer](#)

*Rev. Sci. Instrum.* **84**, 015002 (2013); 10.1063/1.4774054

[Near-Infrared Raman Spectroscopy Using Hollow-Core Photonic Bandgap Fibers](#)

*AIP Conf. Proc.* **1267**, 780 (2010); 10.1063/1.3482806

[A multiplexed fiber Bragg grating sensor for simultaneous salinity and temperature measurement](#)

*J. Appl. Phys.* **103**, 053107 (2008); 10.1063/1.2890156

[Midinfrared sensors meet nanotechnology: Trace gas sensing with quantum cascade lasers inside photonic band-gap hollow waveguides](#)

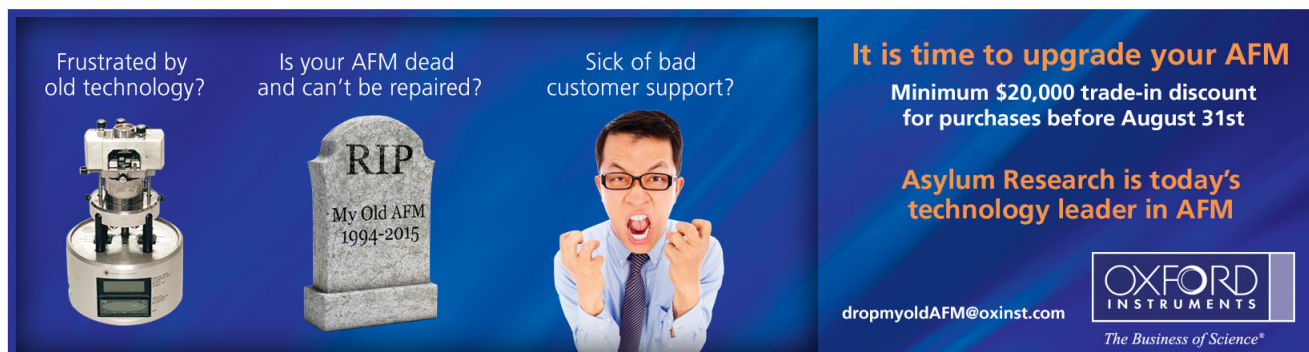
*Appl. Phys. Lett.* **86**, 194102 (2005); 10.1063/1.1925777

[Highly sensitive fiber Bragg grating refractive index sensors](#)

*Appl. Phys. Lett.* **86**, 151122 (2005); 10.1063/1.1904716

---

Frustrated by old technology?      Is your AFM dead and can't be repaired?      Sick of bad customer support?



**It is time to upgrade your AFM**  
Minimum \$20,000 trade-in discount for purchases before August 31st

**Asylum Research is today's technology leader in AFM**

[dropmyoldAFM@oxinst.com](mailto:dropmyoldAFM@oxinst.com)

**OXFORD INSTRUMENTS**  
The Business of Science®

## Photonic bandgap narrowing in conical hollow core Bragg fibers

Fahri Emre Ozturk,<sup>1,2</sup> Adem Yildirim,<sup>1,2</sup> Mehmet Kanik,<sup>1,2</sup> and Mehmet Bayindir<sup>1,2,3,a)</sup>

<sup>1</sup>UNAM-National Nanotechnology Research Center, Bilkent University, 06800 Ankara, Turkey

<sup>2</sup>Institute of Materials Science and Nanotechnology, Bilkent University, 06800 Ankara, Turkey

<sup>3</sup>Department of Physics, Bilkent University, 06800 Ankara, Turkey

(Received 30 April 2014; accepted 8 August 2014; published online 19 August 2014)

We report the photonic bandgap engineering of Bragg fibers by controlling the thickness profile of the fiber during the thermal drawing. Conical hollow core Bragg fibers were produced by thermal drawing under a rapidly alternating load, which was applied by introducing steep changes to the fiber drawing speed. In conventional cylindrical Bragg fibers, light is guided by omnidirectional reflections from interior dielectric mirrors with a single quarter wave stack period. In conical fibers, the diameter reduction introduced a gradient of the quarter wave stack period along the length of the fiber. Therefore, the light guided within the fiber encountered slightly smaller dielectric layer thicknesses at each reflection, resulting in a progressive blueshift of the reflectance spectrum. As the reflectance spectrum shifts, longer wavelengths of the initial bandgap cease to be omnidirectionally reflected and exit through the cladding, which narrows the photonic bandgap. A narrow transmission bandwidth is particularly desirable in hollow waveguide mid-infrared sensing schemes, where broadband light is coupled to the fiber and the analyte vapor is introduced into the hollow core to measure infrared absorption. We carried out sensing simulations using the absorption spectrum of isopropyl alcohol vapor to demonstrate the importance of narrow bandgap fibers in chemical sensing applications. © 2014 AIP Publishing LLC.

[<http://dx.doi.org/10.1063/1.4893594>]

Bragg fibers guide electromagnetic waves using interior dielectric mirrors that enclose the fiber core. Dielectric mirrors, periodically layered materials of different refractive indices, can exhibit omnidirectional reflection at certain bandgaps determined by their layer structure, i.e., by the thicknesses and refractive indices of their material components. Reflection from a dielectric mirror displays similar properties to the diffraction of X-rays from crystal planes, and is therefore called Bragg reflection.<sup>1</sup> The concept of utilizing Bragg reflection in cylindrical waveguides was introduced as early as the late seventies,<sup>2</sup> and first Bragg fibers were produced in the early 2000s.<sup>3</sup> In these fibers, a hollow core is surrounded by alternating layers of a high refractive index chalcogenide glass and a low refractive index polymer. The hollow cores and large photonic bandgaps of Bragg fibers provide a new opportunity for the transmission of light from high intensity sources, such as CO<sub>2</sub> lasers.<sup>3</sup> Bragg fibers are currently under commercial use in minimally invasive laser surgeries.<sup>4,5</sup>

More recently, advantages of using Bragg fibers for chemical sensing applications were realized. The ability to transmit high intensity light, combined with the increased optical path lengths and very small volumes of hollow fiber cores, makes these fibers suitable for trace gas sensing applications.<sup>6</sup> Current approaches for Bragg fiber-mediated chemical detection are based on a variety of mechanisms, such as measuring the infrared absorption of the analyte with a laser source at a specific wavelength,<sup>7</sup> quantifying refractive index changes by measuring shifts in the bandgap of the fiber,<sup>8–10</sup> or placing a chemiluminescent material at the hollow core of the fiber.<sup>11</sup> In our previous studies, we developed an artificial

nose concept utilizing hollow core Bragg fibers as an infrared filter, as well as a gas chamber and a waveguide.<sup>12–14</sup> In this scheme, light from a blackbody source is coupled to the fiber, and its transmitted total intensity is measured with an infrared detector. If there is an overlap between an absorption band of the analyte and the bandgap of the fiber, the transmission is quenched, and this indicates the presence of the analyte. Using an array which consists of fibers with bandgaps at different regions of the mid-infrared allows the targeting of specific absorption bands. The combined response of the fibers enables the selective sensing of analytes using an ordinary blackbody source and an infrared detector. As Bragg fibers were primarily developed for infrared light delivery, recent research has focused on mitigating loss in the infrared region by the enlargement of the omnidirectional bandgap.<sup>15–17</sup> However, typical Bragg fibers with large bandgaps in the mid-infrared region are often responsive to multiple analytes, which may hinder the selectivity of the fiber array.<sup>13,14</sup> Additionally, when the bandgap of the fiber is wide, light is transmitted at the redundant parts of the bandgap, where the transmission is not quenched even after the analyte is introduced to the hollow core of the fiber. This effect weakens the response of the fiber to the analyte. Therefore, Bragg fibers with narrow bandgaps are favorable for chemical sensing and artificial olfaction in terms of improved selectivity and fiber response.

Here, we report the narrowing of the photonic bandgap in conically fabricated Bragg fibers. Conical fibers were produced by thermal drawing under a rapidly alternating load (Figs. 1(a) and 1(b)). A polymer chalcogenide composite preform with alternating layers of arsenic triselenide (As<sub>2</sub>Se<sub>3</sub>) and polyether sulphone (PES) was fabricated with conventional methods.<sup>4,14</sup> The preform was fed in to the fiber tower

<sup>a)</sup>E-mail: bayindir@nano.org.tr

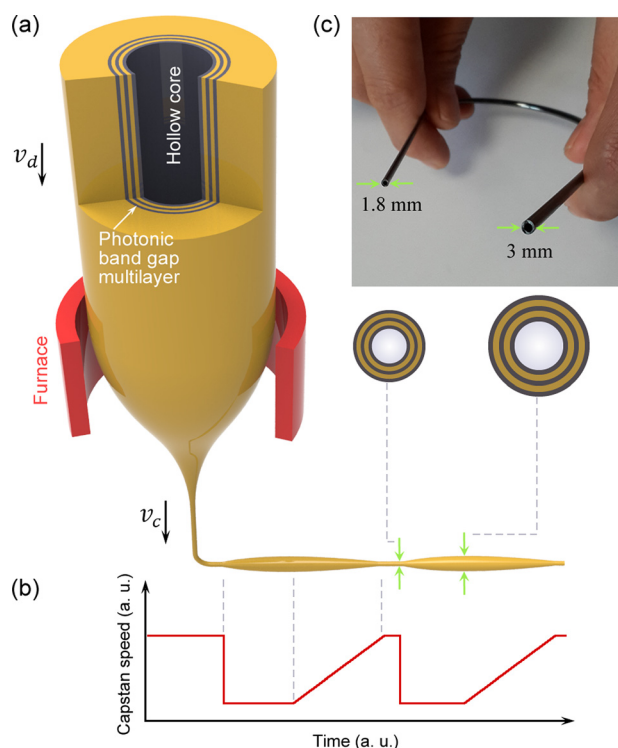


FIG. 1. (a) Thermal drawing of conical hollow core Bragg fibers. The preform is fed into the tower furnace (at 298 °C) with a constant down feed speed  $v_d$ . The macroscopic structure of the preform is scaled down to the micro scale by adjusting the capstan speed (i.e., the drawing speed)  $v_c$ . (b) Step changes in the capstan speed  $v_c$  result in the formation of node structures on the fiber and create conical hollow core Bragg fibers at both ends of the node. (c) A conical fiber with a 40% diameter reduction; the diameter at the base of the conical fiber is 3 mm, whereas the diameter at the tip of cone is 1.8 mm.

furnace at 298 °C with a constant down feed speed  $v_d$  of 8 mm/min under constant load, and scaled down to a diameter of approximately 1.7 mm, where a photonic bandgap range of about 12  $\mu\text{m}$  was reached. At this point, the load on the fiber was changed steeply (in the range of 0.1 to 0.6 kg) by changing the capstan speed (i.e., draw speed)  $v_c$  (Fig. 1(b)). As  $v_c$  decreased, the load on the fiber decreased and the fiber diameter increased gradually. Next,  $v_c$  was increased again with a milder slope to avoid breaking the fiber, and the fiber diameter decreased accordingly. These step changes in load established a node structure on the fiber. Conical fibers were obtained by cutting the node structures in half (Fig. 1(c)). Multiple succeeding nodes with controlled thicknesses can be introduced to the fiber; therefore, conical Bragg fibers with desired lengths and diameter reduction percentages can be produced. A conical fiber with a diameter reduction of 40% is shown in Figure 1(c).

Figure 2 shows the gradual narrowing of the bandgap as light is guided along the conical fiber. The transmission spectrum of a 235 mm conical fiber was compared to transmission spectra measured after segments of certain lengths were cut from the fiber. Four segments cut from a conical fiber and their respective dielectric mirror structures are shown in Figure 2(a). Cross sectional samples from each segment were examined with a scanning electron microscope (SEM) to analyze their dielectric layer thicknesses. A multilayer period gradient starting from  $\Lambda_1 = 2.82 \mu\text{m}$  and ending

at  $\Lambda_4 = 2.50 \mu\text{m}$  was established on a 235 mm long fiber, which corresponds to a decrease of approximately 11% in dielectric layer thicknesses (Fig. 2(a)). Transmission spectra taken after cutting each segment from the thin end of the fiber are shown in Figure 2(b). For the experiments, infrared light from the broadband source of a Fourier transform infrared (FTIR) system was coupled to the fiber, and the transmission spectrum was measured with the externally used DLATGS (deuterated L-alanine-doped triglycine sulfate) detector of the FTIR system. In the first column of Figure 2(b), the transmission spectrum taken from a 50 mm length of fiber after all three pieces were cut from the conical fiber is shown in red spectrum. The top curve in Fig. 2(b) shows the transmission of PES, and the quenching of the photonic bandgap at around  $850 \text{ cm}^{-1}$  is due to the absorption of the polymer. It should be noted that the absorption of polymer layers at mid-infrared region can be avoided with an all-chalcogenide multilayer structure, but an all-chalcogenide Bragg fiber is yet to be fabricated.<sup>18</sup> The second column shows the transmission spectrum of a 90 mm length of fiber taken after cutting two pieces. Similar spectra are given for the third (one segment removed) and fourth (no segments removed) columns. In the spectrum taken from the whole length of the fiber (4th column of Figure 2(b)), the bandgap of the fiber was narrowed to approximately half of the initial bandwidth.

To explain the principles underlying the bandgap narrowing in conical fibers, we carried out simulations of reflection from two dielectric mirror structures with slightly different multilayer periods and consecutive reflections from both of the structures (Fig. 3(a)). Implemented codes solve the reflectance of the periodic multilayer structures analytically for transverse electric (TE) and transverse magnetic (TM) polarizations using the transfer matrix method (TMM).<sup>1</sup> Averages of TE and TM mode transmissions were taken to calculate the overall fiber transmission in all simulations. Figure 3(a) shows the reflectance spectra of two dielectric mirror structures (initial and final) with multilayer periods of  $\Lambda_i = 2.6 \mu\text{m}$  and  $\Lambda_f = 2.3 \mu\text{m}$ , respectively, where multilayer periods are approximately 11% different. The reflectance spectrum generated by consecutive reflections from the initial and final dielectric mirror structures was also simulated using TMM and is shown in green. In the case of consecutive reflections, only wavelengths reflected from both structures remain and the allowed photonic bandgap is at the overlap of reflectances of the initial and final structures. In Figure 3(a), only the case of normal angle of incidence was studied and material absorptions were not taken into account for clarity. Figure 3(b) shows the allowed omnidirectional bands along the conical fiber as a function of diameter reduction percentage. For simulating the bandgap narrowing along the conical fiber, consecutive reflections from linearly decreasing multilayer periods were calculated with TMM. Omnidirectional reflection bands were obtained by taking the average of intensities for each angle of incidence. The gradual reduction of diameter introduced a gradient of interior dielectric layer thicknesses along the conical fibers. As the multilayer period decreased along the fiber, longer wavelengths of the initial bandgap were no longer omnidirectionally reflected and exit through the



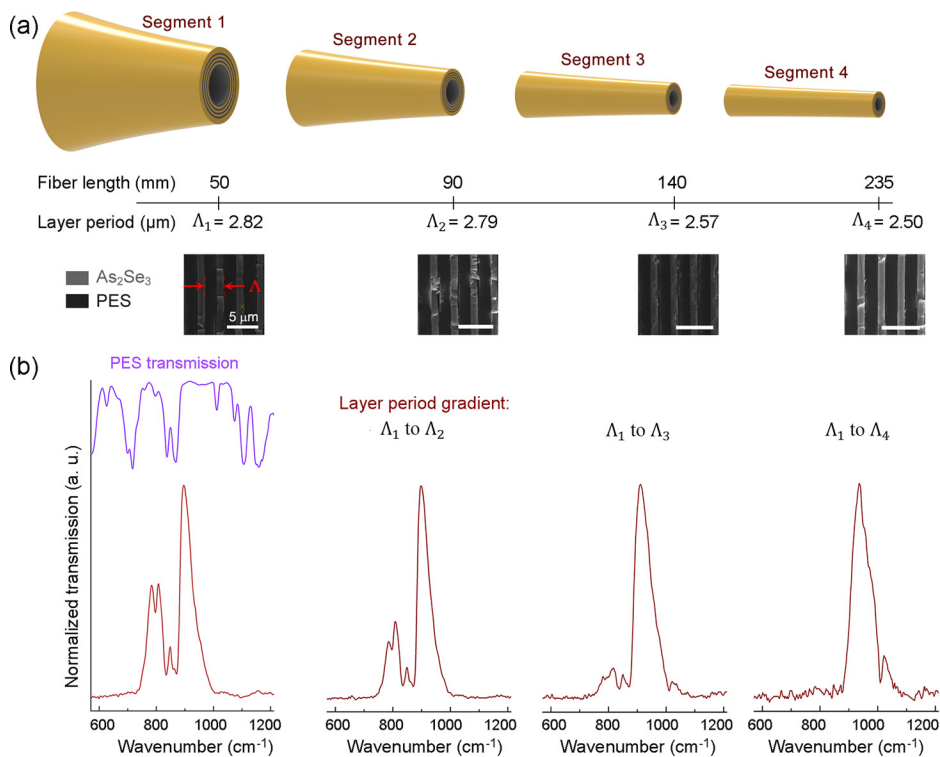


FIG. 2. (a) Segments of a conical hollow core Bragg fiber and scanning electron micrographs of their respective dielectric mirror structures. The dielectric mirror period decreases gradually from  $\Lambda_1 = 2.82 \mu\text{m}$  to  $\Lambda_4 = 2.5 \mu\text{m}$  along the 235 mm fiber (scale bar:  $5 \mu\text{m}$ ). (b) Transmission spectra taken after cutting each segment off the fiber. The spectrum in the first column is taken from a section comprising 50 mm of fiber from the base of the cone, with a dielectric mirror period  $\Lambda_1 = 2.82 \mu\text{m}$ . The spectrum in the second column is taken from a section comprising a 90 mm length of fiber with a dielectric mirror gradient of  $\Lambda_1 = 2.82 \mu\text{m}$  to  $\Lambda_2 = 2.79 \mu\text{m}$ . Spectra in the third and fourth columns were taken from sections of 140 and 235 mm, respectively. The purple spectrum is the transmission of polyether sulphone.

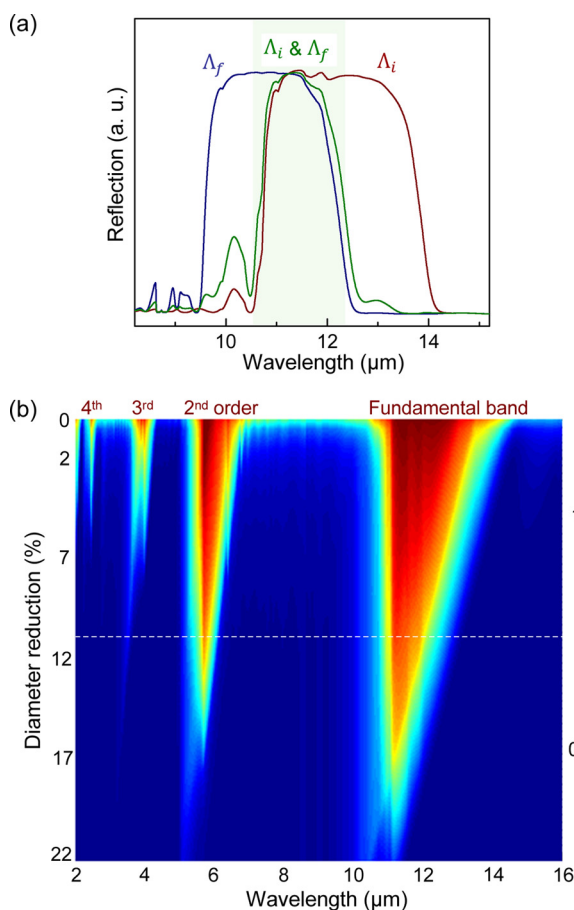


FIG. 3. (a) Transfer matrix method simulations for reflections from two dielectric mirror structures (initial and final) with dielectric mirror periods of  $\Lambda_i = 2.6 \mu\text{m}$  (red line) and  $\Lambda_f = 2.3 \mu\text{m}$  (blue line), and successive reflections from initial and final structures (green line). (b) TMM simulation for the narrowing of the photonic bandgap in conical Bragg fibers as a function of diameter reduction percentage. White dashed line marks a diameter reduction percentage of 11%, matching the fibers characterized in Figure 2.

cladding. The fundamental band (centered at around  $12 \mu\text{m}$ ) is narrowed as the light is guided along the conical fiber. Higher order bands narrow in a similar fashion and disappear after diameter reductions of 5%, 7%, and 17% for 4th order, 3rd order and 2nd order photonic bandgaps, respectively. The fundamental band also virtually vanishes at a diameter reduction of around 22%, where the initial multilayer structure reflectance at the base of the fiber no longer overlaps with the reflectance at the tip. White dashed line marks 11% diameter reduction, a more than twofold narrowing in the omnidirectional band is seen which agrees with the measurements shown in Figure 2(b).

To further verify the proposed narrowing mechanism, we took transmission measurements from two standard (conventional cylindrical) Bragg fibers and one conical fiber. The diameters of the two standard fibers were chosen so that they exactly match with the two ends of the conical fiber, and all three fibers were 260 mm in length. Normalized transmission spectra of the fibers are shown in Figure 4(a). One of the standard fibers had a layer period of about  $2.8 \mu\text{m}$ , and the other had a layer period of  $2.3 \mu\text{m}$ . The conical fiber had a layer period gradient ranging between these two values ( $2.8 \mu\text{m}$  to  $2.3 \mu\text{m}$ ) along its length. The transmission spectrum of the conical fiber is at the overlap of the two standard fibers' transmission bands, as suggested by the simulations in Figure 3. Additionally, the 2nd order bands of the thick and thin standard fibers are observable at around  $2750 \text{ cm}^{-1}$  and  $3250 \text{ cm}^{-1}$ , respectively, but the conical fiber has no 2nd order band, which was also predicted through the simulations. Layer thicknesses of the standard fibers were measured as  $d_1 = 1.11 \mu\text{m}$ , and  $d_2 = 1.71 \mu\text{m}$  for  $\text{As}_2\text{Se}_3$  and PES, respectively, for the thick fiber; and  $d_1 = 0.93 \mu\text{m}$ , and  $d_2 = 1.38 \mu\text{m}$  for the thin fiber. Simulations carried out with these multilayer parameters, which also take angle dependency of reflections and dielectric material absorptions into account,

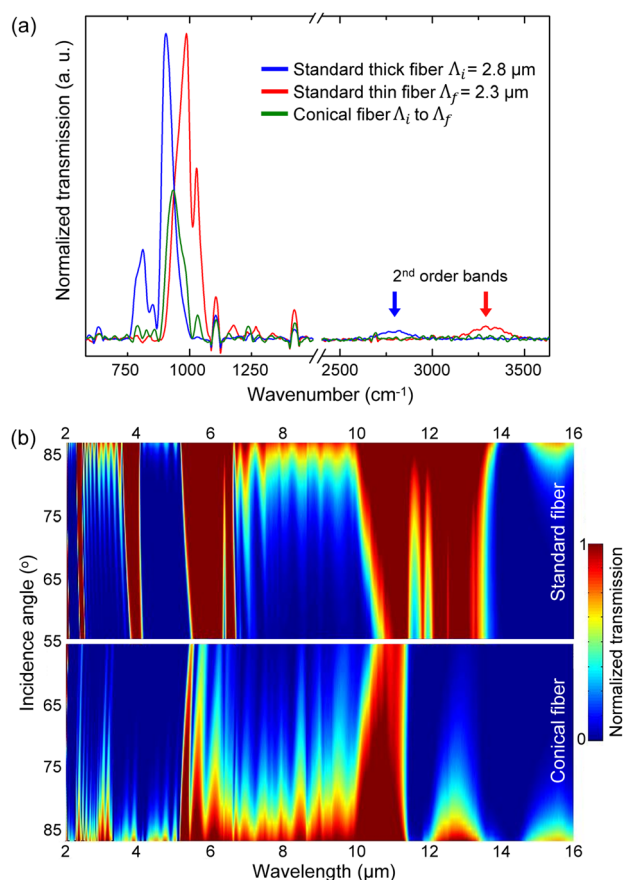


FIG. 4. (a) Measured transmission spectra of two standard Bragg fibers: one with a large diameter (blue line) and the other with a smaller diameter (red line), and a conical Bragg fiber. The conical fiber has a dielectric mirror period gradient between the dielectric mirror periods of the thick and thin standard fibers ( $\Lambda_i = 2.8\mu\text{m}$  to  $\Lambda_f = 2.3\mu\text{m}$ ). The transmission spectrum of the conical fiber is at the overlap of the two standard fibers. In addition, the 2nd order band is absent in the conical fiber, though it exists at wavenumbers around  $2750\text{ cm}^{-1}$  and  $3250\text{ cm}^{-1}$  for standard fibers. (b) Simulations for the thick standard fiber (upper part) and conical fiber (lower part) that take angle dependency of reflections and material absorptions into account.

are shown in Figure 4(b). The upper part of the figure shows the angle dependent photonic bandgap of the thick standard fiber, and the lower part shows that of the conical fiber. The photonic bandgap of the conical fiber was obtained by simulating the consecutive reflections from the multilayer structures of the thick and thin standard fibers with TMM. It should be noted that this approach does not take account for the effect of fiber thickness profile on the bandgap. A more precise calculation of the bandgap requires the use of more rigorous models that take fiber geometry into account.<sup>19</sup> The fundamental photonic band is significantly narrowed for all angles of incidences in the conical fiber, and higher order bands also tend to disappear accordingly.

We studied the sensing performance of conical fibers using isopropyl alcohol (IPA) detection simulations. The measured absorption spectrum of IPA vapor was used to calculate the response of fibers as a function of diameter reduction percentage along the fiber. Transmission spectra of conical fibers with diameter reduction percentages ranging from 0% to 24% were simulated using TMM, and the response of each fiber was calculated as  $((I_0 - I)/I_0) * 100$ , where  $I_0$  is the total transmitted intensity in the absence of

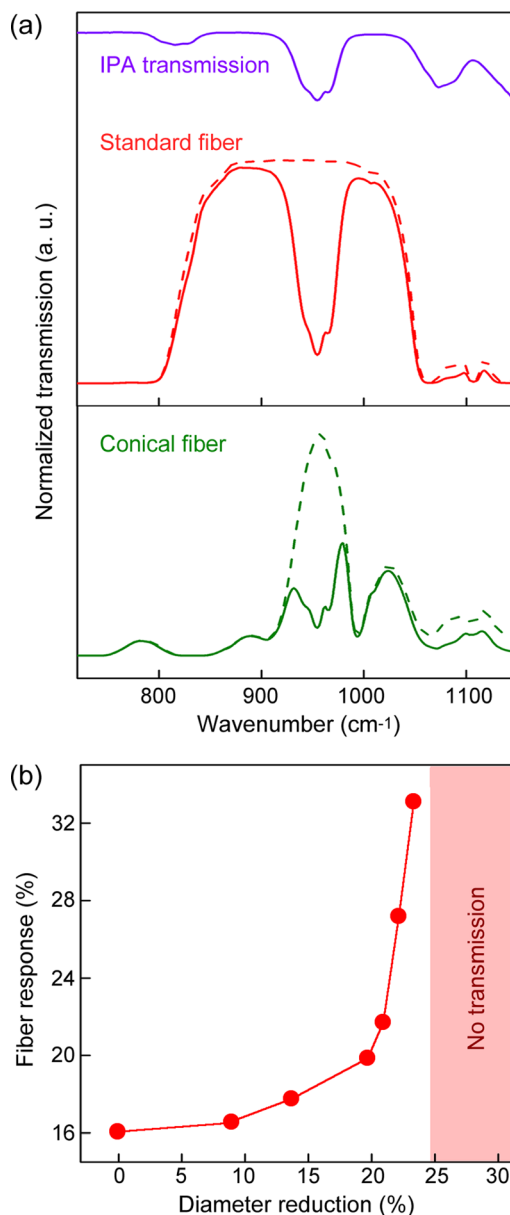


FIG. 5. Simulated responses of standard and conical hollow core Bragg fibers to isopropyl alcohol vapor. (a) Transmission of the standard and conical fibers before (dashed line) and after (solid line) the introduction of IPA. The purple line is the transmission spectrum of IPA vapor. Transmission is strongly quenched after the introduction of the analyte for the conical fiber, whereas quenching is weak for the standard fiber due to the wide transmission band. (c) Fiber response;  $((I_0 - I)/I_0) * 100$ , as a function of diameter reduction percentage, where  $I_0$  is the total transmitted intensity before analyte introduction and  $I$  is the intensity after analyte introduction. There is an exponential increase of fiber response with decreasing cone diameters.

the analyte and  $I$  is the intensity following analyte introduction. Figure 5(a) shows representative transmission spectra of a standard fiber without diameter reduction and a conical fiber with a diameter reduction of about 24%, before and after the introduction of the analyte. The transmission of the fibers was quenched at wavenumbers around  $975\text{ cm}^{-1}$ , where the absorption band of IPA was overlapped with the photonic bandgap of the fibers. The quenching in the conical fiber is much more pronounced, as a large part of the wide bandgap of the standard fiber is redundant, i.e., light is transmitted at this region even in the presence of IPA. Figure 5(b) compares the responses of fibers with different degrees of

conicality. The response of the fibers increases exponentially with increasing diameter reduction percentages. The fundamental band of the conical fibers vanishes completely for diameter reduction percentages larger than 24%. It should also be noted that wide bandgaps and higher order bands may respond to chemicals other than the intended analyte and result in non-selective detection.<sup>13,14</sup> Therefore, the ability to tune the width of the fundamental band and to eliminate undesired higher order bands in hollow core photonic bandgap fibers is advantageous for high-selectivity chemical sensing efforts.

In conclusion, we engineered the bandgap of Bragg fibers by introducing a gradient of interior dielectric mirror layer thicknesses throughout the fiber. The gradual change of the dielectric multilayer period along the length of the fiber was established in conical Bragg fibers, which were produced by altering the load on the fiber rapidly during thermal drawing. The fundamental photonic bandgap was narrowed around twofold, and higher order bands were eliminated in conical Bragg fibers with a diameter reduction of 11%. The principles underlying the bandgap narrowing phenomenon were explained by employing TMM to simulate reflectance spectra from successive dielectric mirrors with gradually changing layer periods. Due to the interior multilayer period gradient of the conical fiber, the light guided within the structure encountered dielectric mirrors with slightly shifted reflection bands at each reflection point, and the photonic bandgap narrowed with each reflection. The photonic bandgap of the conical fiber was therefore in the overlap of dielectric mirror reflectance spectra at both extremes of the gradient. We expect the proposed method to provide additional flexibility in the design of Bragg fibers and a better performance in trace gas sensing or artificial nose technologies that utilize hollow core photonic bandgap fibers. Lastly, the same principles can be employed for the introduction of structure gradients in other types of fibers, which could lead to the emergence of interesting fiber characteristics.

F. E. O. Wishes to thank A. Eren Öztürk for his help in the modelling of 3D figures, Tamer Doğan, Erol Özgür, and

Urandelger Tuvshindorj for their fruitful discussions, Murat Dere for his assistance in the preparation of preforms and Alper Devrim Özkan for improving the use of English in the manuscript. This work was partially supported by TUBITAK under the Project No. 113T069. The research leading to these results has received funding from the European Research Council under the European Union's Seventh Framework Programme (FP/2007-2013)/ERC Grant Agreement No. 307357. M.B. acknowledges partial support from the Turkish Academy of Sciences (TUBA).

- <sup>1</sup>P. Yeh, *Optical Waves in Layered Media* (Wiley-Interscience, Hoboken, New Jersey, 1998).
- <sup>2</sup>P. Yeh, A. Yariv, and E. Marom, *J. Opt. Soc. Am.* **68**, 1196 (1978).
- <sup>3</sup>B. Temelkuran, S. D. Hart, G. Benoit, J. D. Joannopoulos, and Y. Fink, *Nature* **420**, 650 (2002).
- <sup>4</sup>A. F. Abouraddy, M. Bayindir, G. Benoit, S. D. Hart, K. Kuriki, N. Orf, O. Shapira, F. Sorin, B. Temelkuran, and Y. Fink, *Nat. Mater.* **6**, 336 (2007).
- <sup>5</sup>R. W. Ryan, T. Wolf, R. F. Spetzler, S. W. Coons, Y. Fink, and M. C. Preul, *J. Neurosurg.* **112**, 434 (2010).
- <sup>6</sup>L. C. Shi, W. Zhang, J. Jin, Y. Huang, and J. D. Peng, *Opt. Sens. Biophotonics II* **7990**, 799008 (2011).
- <sup>7</sup>C. Charlton, B. Temelkuran, G. Dellemann, and B. Mizaikoff, *Appl. Phys. Lett.* **86**, 194102 (2005).
- <sup>8</sup>D. Chen, T. J. Yang, J. J. Wu, L. Shen, K. L. Liao, and S. He, *Opt. Express* **16**, 16489 (2008).
- <sup>9</sup>H. Qu and M. Skorobogatiy, *Appl. Phys. Lett.* **98**, 201114 (2011).
- <sup>10</sup>K. J. Rowland, S. Afshar, A. Stolyarov, Y. Fink, and T. M. Monro, *Opt. Express* **20**, 48 (2012).
- <sup>11</sup>A. M. Stolyarov, A. Gumennik, W. McDaniel, O. Shapira, B. Schell, F. Sorin, K. Kuriki, G. Benoit, A. Rose, J. D. Joannopoulos, and Y. Fink, *Opt. Express* **20**, 12407 (2012).
- <sup>12</sup>A. Yildirim, M. Vural, M. Yaman, and M. Bayindir, *Adv. Mater.* **23**, 1263 (2011).
- <sup>13</sup>M. Yaman, A. Yildirim, M. Kanik, T. C. Cinkara, and M. Bayindir, *Anal. Chem.* **84**, 83 (2012).
- <sup>14</sup>A. Yildirim, F. E. Ozturk, and M. Bayindir, *Anal. Chem.* **85**, 6384 (2013).
- <sup>15</sup>A. Husakou and J. Hermann, *Opt. Express* **17**, 3016 (2009).
- <sup>16</sup>D. J. J. Hu, G. Alagappan, Y. K. Yeo, P. P. Shum, and P. Wu, *Opt. Express* **18**, 18671 (2010).
- <sup>17</sup>L. Shang, X. Yang, Y. Xia, and H. Wang, *J. Lightwave Technol.* **32**, 1717 (2014).
- <sup>18</sup>H. E. Kondakci, M. Yaman, O. Koylu, A. Dana, and M. Bayindir, *Appl. Phys. Lett.* **94**, 111110 (2009).
- <sup>19</sup>M. Skorobogatiy, S. A. Jacobs, S. G. Johnson, and Y. Fink, *Opt. Express* **10**, 1227 (2002).